4.A.1 Introduction

Nanoparticles synthesized under constrained environment like micelles are approximately monodispersed and exhibited better luminescence properties. Anionic surfactants like sodium dodecylsulphate (SDS) or cationic surfactant like cetyltrimethylammonium bromide (CTAB) are used for the purpose. The concentration of the surfactant is kept above critical micelle concentration (CMC) to facilitate micelle formation. Micelles act as micro/nano reactors resulting nearly monodispersed nanoparticles. At the end, nanoparticles may be recovered by breaking micelles using super critical CO_2 [1]. Considerable experimental works have been carried out in past few years to understand the role of surfactant in synthesis of nearly monodispersed nanoparticles [2, 3]. For example, Mitra et al. prepared the nanosized ZnS particles in micellar medium of SDS [4]. Mehta et al. prepared colloidal dispersions of ZnS using cationic surfactants cetyltrimethylammonium chloride (CTAC) and cetyltrimethylpyridinium chloride (CPyC) [5]. Murugadoss et al. studied the stabilization mechanism of ZnS nanoparticles using CTAB in aqueous media [6]. The pH maintained during the synthesis directly affects the optical properties of ZnS nanoparticles. For example, Borse et al. synthesized mercaptoethanol passivated ZnS:Pb nanoparticles and correlate the luminescence intensity of the material with the pH of the medium [7]. Ullah et al. synthesized ZnS nanoparticles of two different sizes (3.0 ± 0.5 and 6.5 ± 0.5 nm) in neutral and acidic medium respectively using b-cyclodextrine as stabilizer [8]. They observed different growth processes of nanoparticles at different pH, however, band edge emissions were dominant in both the cases.

In present study, we have synthesized ZnS nanoparticles in SDS micellar medium above critical micelle concentration (CMC) by simple wet chemical method. We have also studied the effect of pH of the reaction medium (acidic or basic) on the optical properties of the as-synthesized nanoparticles in terms of absorbance and photoluminescence. We have also attempted to establish relationship between the crystallinity of the material with its optical performance.

4A.2. Experimental

(a) Materials

Analytical Grade zinc nitrate, sodium dodecylsulphate (SDS), nitric acid and sodium sulphide were purchased from S. D. Fine Chemicals Ltd. Mumbai, India and used as received.

(b) Synthesis of ZnS nanoparticles in basic medium

ZnS nanoparticles were synthesized in SDS solution above CMC at RT. 6 mL aqueous solution of Na2S (1.28 M) and 15 mL aqueous solution of SDS (0.46 M) were mixed and stirred for half an hour to obtain a homogenous solution. To this solution, 11 mL aqueous solution of $Zn(NO_3)_2$ (0.38 M) was added drop wise at the rate of 1 mL/min. At this time, the pH of reaction mixture was increased and become 11.8 remained constant up to the end of reaction. The reaction mixture was continuously stirred for 48 h to obtain homogenous stabilized dispersion. The reaction mixture was centrifuged at 10,000 rpm and washed several times with distilled water to remove the unreacted precursors. The product was dried at 60 °C to obtain ZnS nanoparticles in form of powder material. The dried powder was used for different characterizations.

(c) ZnS nanoparticles synthesized in acidic medium

1.25 g of $Zn(NO_3)_2$ (0.38 M) was dissolved in 11 mL 1.4 M nitric acid and pH was maintained 1.3. The rest of conditions were same as for basic medium.

4A.3. Results and discussion

Powder X-ray Diffraction (XRD)

The X-ray diffraction patterns of as-synthesized nanoparticles in acidic and basic medium are shown in Figure 4A.1. It can be seen that both the samples have similar XRD patterns analogous to JCPDS card No. 65-0309, manifesting cubic zinc blende structure. The XRD patterns manifest three predominant diffraction peaks at 28.6°, 46.6° and 56.2° corresponding to the (111), (220) and (311) planes respectively. The

nanoparticles are free from any impurities as no other prominent peaks were observed. The broadness of the base of the peaks indicates that average particle size is in the nanometer range, calculated using Debye–Scherrer formula to be 10.7 and 11.3 nm (Table 1) for the samples synthesized in the basic and acidic medium respectively [9]. It can be observed that for both the samples, full widths at half maximum (FWHM) values are almost same for all three peaks. FWHM values reflect the particle size of the material, more is the broadening of the peaks, more will be the FWHM and less the particle size. XRD patterns show that both samples possess almost same type of crystalline packing, however, the shape of the peaks correspond to the sample in basic medium is more sharp and clearly resolved from the top portion than in acidic medium suggesting better crystallinity in material.

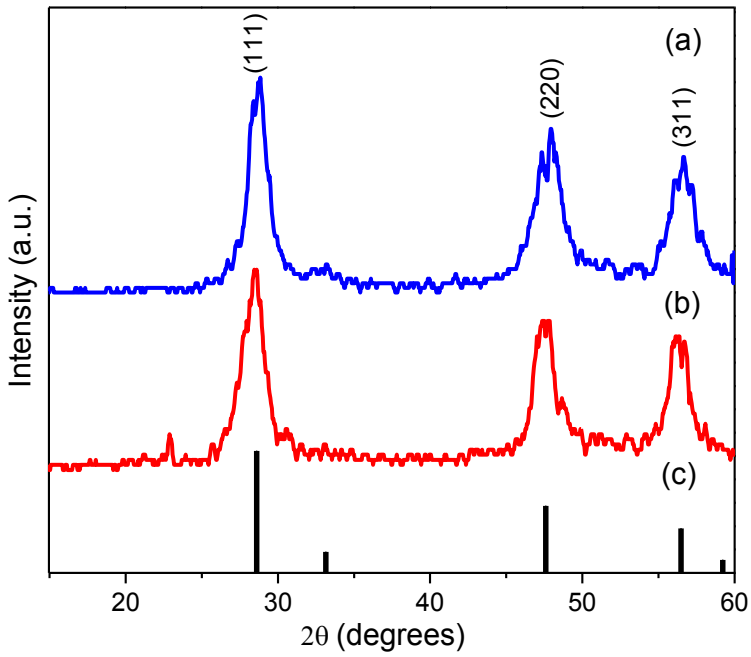

Figure 4A.1 The XRD pattern of ZnS nanoparticles synthesized in the (a) basic medium, (b) acidic medium and (c) standard cubic ZnS (JCPDS card No. 65-0309).

Table 1. Particle size of ZnS nanoparticles synthesized in both the medium.

pH	UV absorption (nm)	E_g (eV)	Particle size calculated using Debye-Scherrer formula (nm)
basic (11.8)	254	4.18	10.7
acidic (1.3)	276	3.83	11.3

Transmission Electron Microscopy (TEM)

The size and shape of the ZnS nanoparticles synthesized in different mediums were studied by TEM (Figure 4A.2). It can be observed that the nanoparticles synthesized in basic medium are highly crystalline having smooth surface and average size 88 nm. The SAED pattern confirms this observation (Figure 4A.2b), also corroborates the argument from XRD patterns. The nanoparticles synthesized in acidic medium were of average 140 nm in size and spherical in shape (Figure 4A.2c). It can be seen that these particles are made of aggregates of small spherical particles of average 8 nm in size. Such type of aggregation induces microcrystallinity in the material, confirmed by SAED pattern (Figure 4A.2d) and also further supported by XRD.

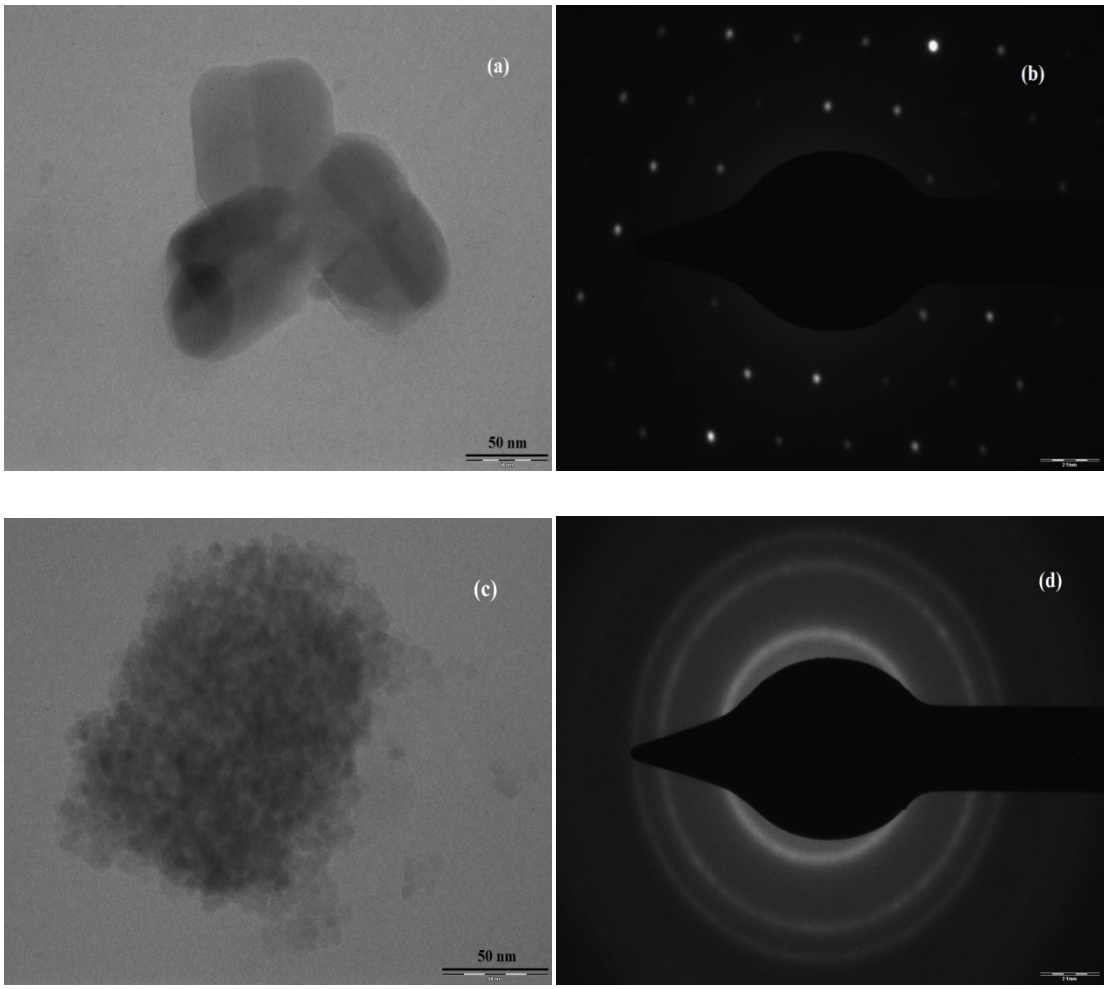

Figure 4A.2 TEM image and SAED pattern of the ZnS nanoparticles prepared in the (a,b) basic medium (c,d) acidic medium.

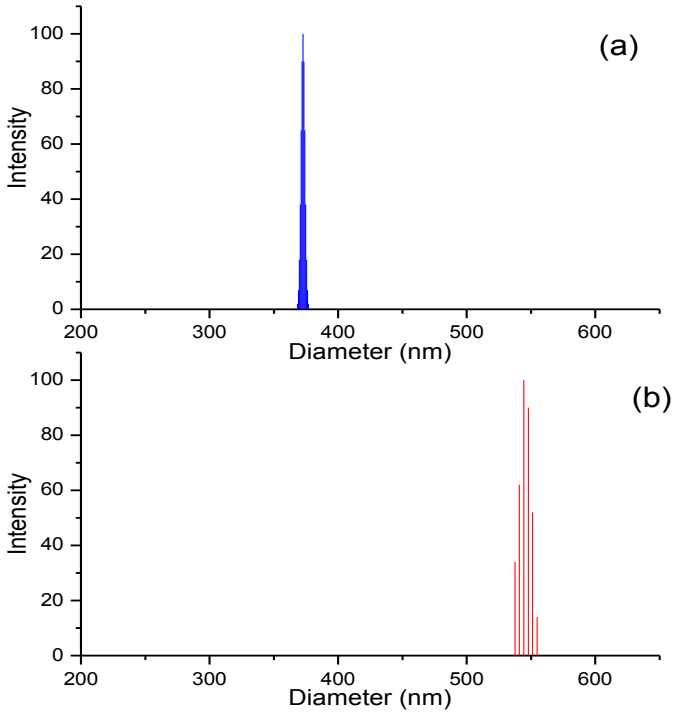

Figure 4A.3 Particle size of ZnS nanoparticles synthesized in (a) basic and (b) acidic medium from Dynamic light scattering.

Table 4A.2 Particle size and zeta potential of ZnS nanoparticles as studied by Dynamic light scattering.

pH	Hydrodynamic diameter (nm)	Zeta potential (ζ) (mV)
12.4	372.7	-9.33
1.3	544.4	+7.82

Dynamic light scattering (DLS) analysis and zeta potential

The particle size of the doped and undoped ZnO nanoparticles was studied by DLS study as shown in Figure 4A.3. The particle diameter of undoped and doped ZnO

nanoparticles was in the range of 300-600 nm as given in Table 2. The surface charges of the nanoparticles were studied by zeta potential (f) measurement. It gives an idea about the electrostatic charge stabilization during the growth of nanoparticles. From Table 1 it can be seen that ZnS nanoparticles from basic medium possess negatively charged surface while those from acidic medium possess positively charged surface. The emergence of a charge on the surface is directly influenced by the presence of counter ions in the medium and the mode of crystallization. The probable mechanism for the formation of negative charge on the surface of ZnS nanoparticles in basic media could be suggested below:

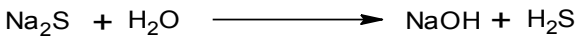

$$Na_2S + H_2O \longrightarrow NaOH + H_2S \quad \text{.....(1)}$$

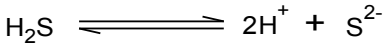

$$H_2S \rightleftharpoons 2H^+ + S^{2-} \quad \text{..... (2)}$$

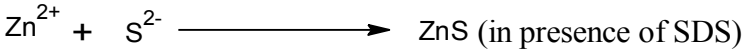

$$Zn^{2+} + S^{2-} \longrightarrow ZnS \text{ (in presence of SDS)} \quad \text{..... (3)}$$

As Na_2S is a salt of weak acid and strong base, the resulting solution becomes basic (eq.1). Due to weak acidic nature, an equilibrium is established between dissociated ions and undissociated H_2S in aqueous medium containing SDS (eq. 2). When Zn^{2+} ions are introduced in a reaction mixture, they react with S^{2-} ions and first nuclei of ZnS are formed. For this reason, the equilibrium of eq. 2 is disturbed and shifted towards right generates more numbers of S^{2-} ions successively adsorbed on the surface of growing ZnS nuclei together with hydroxyl ions produced by eq.1. At one stage of growth the hydrophobicity of the growing particle become sufficient to move in the pockets of SDS micelles for stabilization. These produce a compactness and hence crystallinity in a material. On vigorous centrifugation, the micelles could be broken forming ZnS nanoparticles. When dry powder suspended again in aqueous medium, it shows negative charge due to the adsorbed S^{-2} and OH^- ions (from eq 1).

In case of acidic medium, $Zn(NO_3)_3$ was dissolved in 1.4 M HNO_3. In such condition $Zn(NO_3)_3$ dissociate as :

$$Zn(NO_3)_2 + H_2O \rightleftharpoons Zn(OH)_2 + HNO_3 \quad \text{..... (4)}$$

In presence of excess nitric acid in the medium reaction (4) is driven far left and Zn^{+2}ions combines with S^{-2} ions to form ZnS nuclei. Now, the equilibriums of eq. (2) as well as eq. (4) would be shifted towards right side. However, the number of Zn^{+2} ions are more than that of S^{-2} ions due to easy dissociation of $Zn(NO_3)_3$ than H_2S. Consequently, during crystal growth process Zn^{+2} ions preferentially adsorbed on the growing surface and the surface charge becomes positive. During overall reaction in both acidic and basic medium, SDS acts as a stabilizer, controls the nucleation and growth of ZnS by preventing the aggregation of nanoparticles.

Optical study

The absorption spectra of both samples are shown in Figure 4A.4 The absorption spectra shows sharp onset shift towards higher energy from acidic to basic medium. The onset is followed by sharp absorption edge due to narrow size distribution of particles. It can be observed from Table 1 that the absorption edge is blue shifted from the bulk value (335 nm). The large blue shifting in the band edge in basic medium indicates broadening of the band gap and discreteness of the bands. These increase the life-time of excitons at room temperature resulting in sharp band-edge emission in UV spectrum. The absorption spectrum (Figure 4A.3b) in acidic medium shows two maxima at 215 and 248 nm. Dustan et al explained these emissions due to Zn^{+2} ion excess (which support our previous explanation about zeta potential in acidic medium) [10]. Generally, such type of behavior is observed because of interstitial vacancies and lattice defects present in the material.

The band gap energy was calculated from the plot of $(\alpha h\nu)^2$ Vs hν extrapolating on the hν axis, as shown in Figure 4A.5. The values are found to be 4.18 and 3.83 eV (Table1) for samples synthesized in basic and acidic medium respectively. Equation 5 was used for the purpose.

$$(\alpha h\nu)^2 = A\,(h\nu - E_g) \quad \text{.....(5)}$$

Where, α, hν, E_g and A are the absorption coefficients, incident photon energy, band gap energy of the nanoparticles and constant respectively.

The band gap values are larger than the bulk ZnS (3.66 eV). This is due to quantum confinement effect in a small volume [11]. Further, it can be observed that the band gap in basic medium (4.18 eV) is more than that in acidic medium (3.83 eV). This is due to the difference in crystallinity of the material. From the study of UV absorption spectrum, it can be assumed that basic medium favors crystallinity in a material leads to broadening of the band gap in turn sharp band edge emissions. To confirm the assumption, photoluminescence (PL) studies were carried out. It was observed that both samples show excitation maxima at 285 nm. Therefore, PL spectra for both of the samples were obtained at excitation wavelength of 285 nm (Figure 4A.6). It can be seen that on excitation, multiple emission processes initiated in the material. The emission spectrum may be divided into two regions. Firstly in UV region, the intensities of two maxima at 330 and 350 nm are higher for the sample synthesized in basic medium than those in acidic medium. These peaks are due to band to band [12] and near band-edge transitions [13]. If the material synthesized in basic medium possesses high crystallinity then only the high intensity of emission possible due to discreteness in band gap support our assumption. However, the second part of the spectrum of the same sample is in visible region having lower intensity than acidic one. Such emissions are due to defects, vacancies and extra ions presents at interstitial sites. Surface defects are excellent sites for radiative recombination of electron–hole pair results into emission in visible region. The maximum at 470 nm is due to Zn vacancy [14] and those at 485 nm and 492 nm are due to Zn and S ions having dangling bonds. The sample synthesized in acidic medium possesses more defects and interstitial sites than that in basic medium resulting higher intensity of peaks in visible region of PL spectrum.

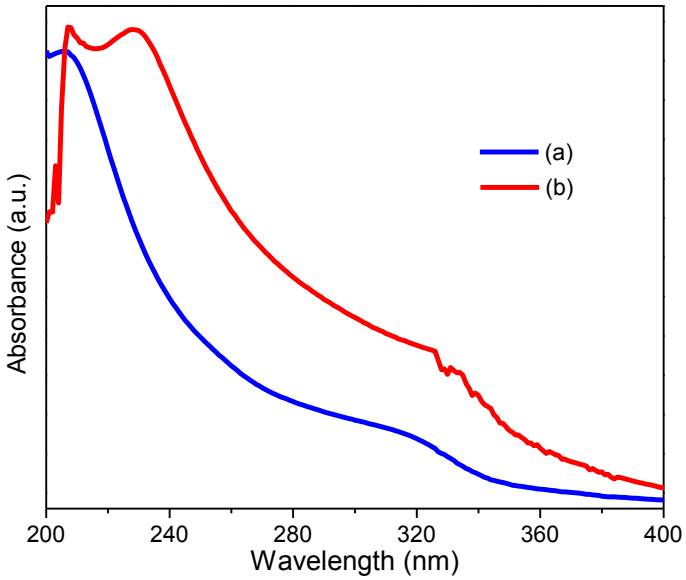

Figure 4A.4. Absorption spectra of ZnS nanoparticles synthesized in (a) basic and (b) acidic medium.

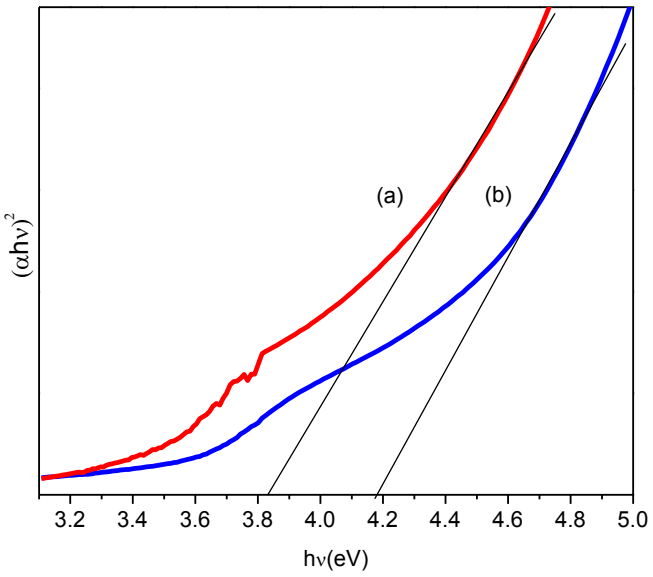

Figure 4A.5. Plot of $(\alpha h\nu)^2$ vs hν of ZnS nanoparticles synthesized in (a) basic and (b) acidic medium.

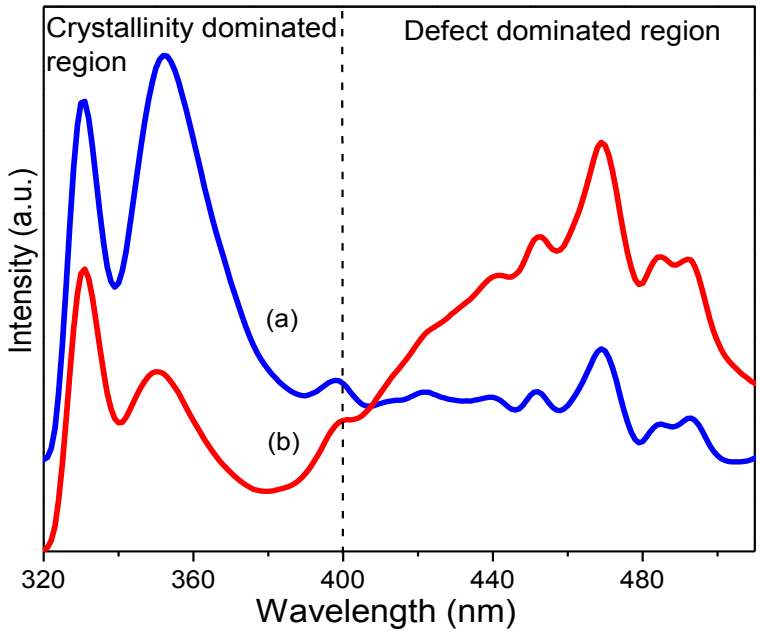

Figure 4A.6. Emission spectra of nanoparticles synthesized in (a) basic and (b) acidic medium.

Fourier Transform Infrared Spectroscopy (FT-IR)

To understand the induction of crystallinity in a basic medium, it is necessary to study the interaction among the ligands (free ions and water molecules) and surfaces of the growing nanoparticles. FTIR spectroscopy is one of the best tools for the purpose. Figure 4A.7 compares the FTIR spectra of ZnS nanoparticles synthesized in acidic and basic medium and the wave numbers of main peaks in the spectra are listed in Table 3. It can be seen that the spectrum of the sample from basic medium possesses sharp peaks than that in acidic medium between the regions 3600–1600 cm^{-1} indicates proper alignment of adsorbed ligands (water, H^+ or OH^-) on the surface and are in ordered and densely packed monolayer than partial double layer [15]. The broad peaks in the region 3000–3500 cm^{-1} are due to stretching vibrations of liquid water with distorted H-bonding. Bending vibration of water d (HOH), however, appear at 1628 cm^{-1} for basic and 1617 cm^{-1} for acidic medium ZnS nanoparticles, instead of

1638 cm^{-1} for pure water. These blue shifting of the peaks indicates molecular water bound electrostatically to the surface of nanoparticles. The presence of SDS adsorbed on the surface of nanoparticles can also be confirmed by FTIR spectroscopy. The broad H-bonding peak at 3413 cm^{-1} for basic medium is sharper and blue shifted than that for acidic medium at 3363 cm^{-1} suggesting high crystallinity of the material. Gilbert et al. observed that capping nanocrystals surfaces such that both surface anions and cations are fully bonded will produce the most crystalline nanoparticles [16]. In our case, capping agent SDS, water molecules and OH_/H+ ions present in the medium electrostatically adsorbed on the surface of nanoparticles and satisfy almost all dangling bonds make them stable and more compact resulting into higher crystallinity. In basic medium, besides water and SDS, OH^- ions strongly interact with the surface make it electrostatically more stable and compact should be the reason for favoring crystallinity in basic medium.

Table 3. FTIR frequencies indicating the existence of SDS on the surface of ZnS nanoparticles.

IR frequency (cm^{-1})	**Inference [17, 18]**
660	Zn-S vibration.
459 and 537	S-S or S-O interaction.
1008	S–O–C stretching.
1132	S-O stretching vibration due to presence of sulphate ions from the adsorbed SDS.
1384	Bending vibrations of $-CH_2-$.
1450	$-CH_2-$ scissoring.
2921	asymmetric methylene stretches hydrocarbon chain tail of the adsorbed SDS

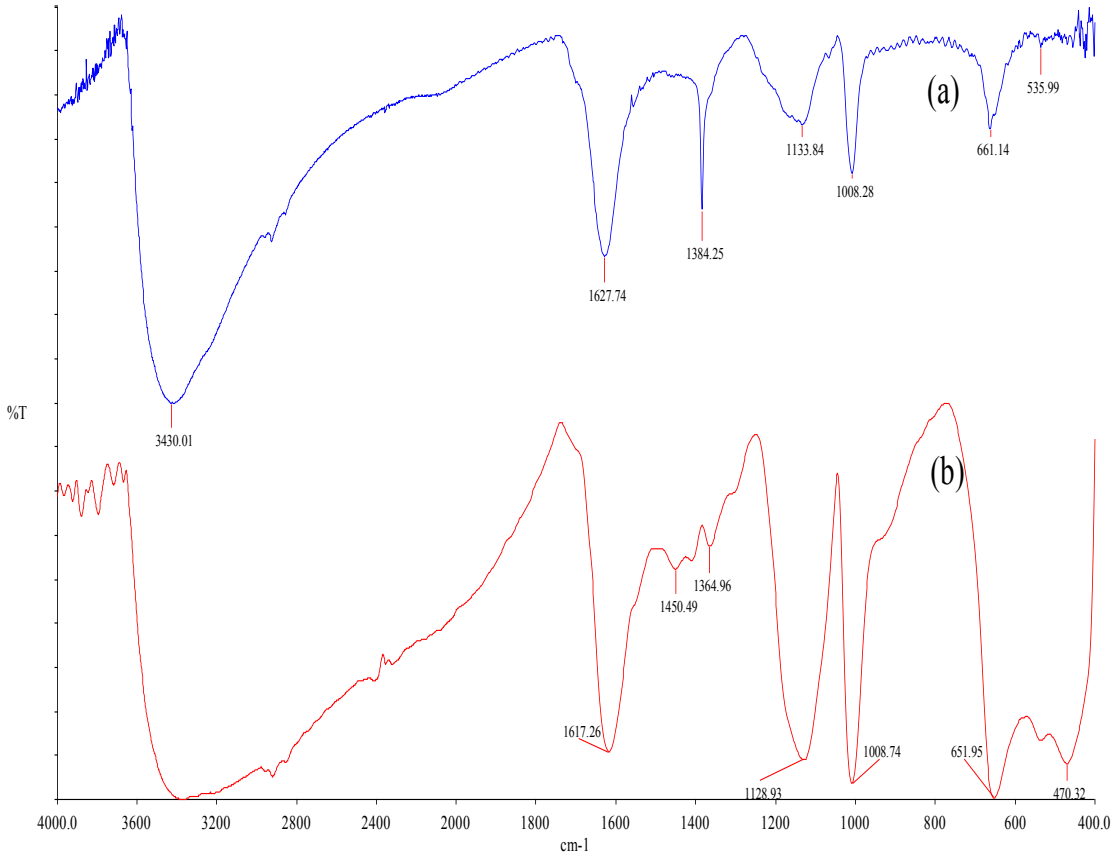

Figure 4A.7. FTIR spectra of ZnS nanoparticles synthesized in (a) basic and (b) acidic medium.

4.1.4. Conclusion

ZnS nanoparticles are synthesized in acidic and basic medium using SDS as a capping agent. The present study allows us to conclude: (1) optical performance of the ZnS nanoparticles can be tuned by selecting proper pH of the reaction medium. (2) Basic medium induces crystallinity in a material due to electrostatic interaction of free OH^-, S^{-2} ions, water and capping agent with the surface of the growing ZnS nanoparticles, most of the dangling bonds are satisfied resulting into compact packing of the material responsible for higher crystallinity. (3) Acidic medium favors porous and microcrystalline material. (4) Due to higher crystallinity band-edge emission in UV region is dominated in basic medium while in acidic medium due to large number of defects and vacancies, emissions in visible region are dominated.

References

[1] J. Zhang, B. Hand, J. Liu, X. Zhang, Z. Liu, J. He, *Chem. Commun.* **2001**, 2724.

[2] R. Maity, K.K. Chattopadhay, *Nanotechnology* **2004,**15. 812.

[3] Y. Yang, J. Huang, S. Liu, J. Shen, *J. Mater. Chem.* **1997**, 7, 1969.

[4] D. Mitra, I. Chakraborty, S.P. Moulik, *Colloid J.* **2005**, 67, 445.

[5] S.K. Mehta, S. Kumar, S. Chaudhary, K.K. Bhasin, *Nanoscale Res. Lett.* **2009**, 4, 1197.

[6] A. Murugadoss, A. Chattopadhyay, *Bull. Mater. Sci.* **2008**, 31, 533.

[7] P.H. Borse, W. Vogel, S.K. Kulkarni, *J. Colloid Interface Sci.* **2006**, 293, 437.

[8] M.H. Ullah, I. Kim, C.-S. Ha, *Mater. Lett.* **2007**, 61, 4267.

[9] R. Jenkins, R.L. Snyder, *Introduction to X-ray Powder Diffractometry*, John Wiley and sons, NewYork, **1996**.

[10] D.E. Dunstan, A. Hagfeldt, M. Almgren, H.O.G. Siegbahn, E. Mukhtar, *J. Phys. Chem.* **1990**, 94, 6797.

[11] L.E. Brus, *J. Chem. Phys.* **1984**, 80, 4403.

[12] J.X. Ding, J.A. Zapien, W.W. Chen, Y. Lifshitz, S.T. Lee, X.M. Meng, *Appl. Phys. Lett.* **2004**, 85, 2361.

[13] N. Chestnoy, R. Hull, L.E. Brus, *J. Chem. Phys.* **1986**, 85, 2237.

[14] W.-H. Zhang, J.-L. Shi, H.-R. Chen, Z.-L. Hua, D.-S. Yan, *Chem. Mater.* **2001**, 13, 648.

[15] P. Jeevanandam, K.J. Klabunde, *Langmuir* **2002**, 18, 5309.

[16] B. Gilbert, F. Huang, Z. Lin, C. Goodell, H. Zhang, J.F. Banfield, *Nano Lett.* **2006**, 6, 605.

[17] D.A. Reddy, G. Murli, B. Poornaprakash, R.P. Vijayalakshmi, B.K. Reddy, *Appl. Surf. Sci.* **2012**, 258, 5206.

[18] X. Wang, Y. Du, H. Liu, *Carbohydr. Polym.* **2004**, 56, 21.

4B.1 Introduction

The surfactant molecules form micelle when dissolved in water or oil at and above Critical Micelle Concentration (CMC), which can be used as a nano-reactor for the synthesis of nanoparticles. The shape of the micelle can be adjusted by changing the experimental parameters such as temperature, concentration, polarity of the solvent etc. Sodium bis(2-ethylhexyl)sulfosuccinate (AOT) is an anionic surfactant with a double hydrophobic chains, which forms micelles of different shapes such as spheres, rods, ellipsoids, disks and layered structures in the ternary (AOT/non-polar sovent/water) system depending on the experimental parameters such as concentration, temperature, co-surfactant etc [1]. Xu et al. synthesised ZnS nanorods and nanoparticles in w/o microemulsion [2].

Doped ZnS material finds application in optical displays, photocatalysis and spintronics. Bi et al. reported blue emission from Co doped ZnS nanocrystals [3]. Kang et al. reported room-temperature ferromagnetism in Mn/Fe-doped and co-doped ZnS nanostructures [4].

In the present work, we have synthesized Fe^{2+}, Co^{2+}, Ni^{2+} , Mn^{2+} doped and undoped ZnS nanoparticles by using oil-in-water (o/w) microemulsion using sodium bis(2-ethylhexyl)sulfosuccinate (AOT) and 1-butanol as the surfactant and oil phase respectively. The effect of dopant ions and anions (of precursors) on the optical properties and surface stabilization of the host material are studied.

4B.2. Experimental

(a) Materials

Analytical Grade zinc acetate $Zn(CH_3COO)_2.2H_2O$, zinc chloride $ZnCl_2$, ferrous sulphate $FeSO_4.7H_2O$, sodium sulphide $Na_2S.xH_2O$, 1-butanol and sodium bis(2-ethylhexyl)sulfosuccinate (AOT) $C_{20}H_{37}NaO_7S$, Ferrous sulphate ($FeSO_4.7H_2O$), cobalt chloride ($CoCl_2.6\ H_2O$), nikel acetate ($Ni(CH_3COO)_2.4H_2O$) and manganese

acetate ($Mn(CH_3COO)_2.4H_2O$) were obtained from SD Fine Chemie Pvt. Ltd. Mumbai, India and used as received.

(b) Synthesis procedure

The method applied for the synthesis of doped and undoped ZnS nanoparticles was modified method of Li et al. for the ZnO hexagonal disks using oil-in-water microemulsion with AOT/1-butanol/water system [5]. Oil-in-water microemulsion of Zn^{2+} and Co^{2+} was prepared by using 100 ml $Zn(NO_3)_2.6H_2O$ (2.5×10^{-3} mol), $CoCl_2.6H_2O$ (1.38×10^{-3} mol) and 10 ml 0.1M AOT in 1-butanol. To the Zn^{2+} and Co^{2+} containing emulsion, liquor NH_3 was added in the ratio, NH_3: $Zn(NO_3)_2$ as 4:1. Similarly S^{2-} containing emulsion was prepared by using aqueous solution of Na_2S (0.05M or 5.0×10^{-3} mol). The S^{2-} ions containing emulsion was added dropwise to the Zn^{2+} and Co^{2+} ions containing emulsion. The resulting reaction mixture was allowed to stir at room temperature (35°C) for 5 days. A resulting dispersion was centrifuged, washed with distill water and absolute ethanol three times. The product was dried at 60°C to obtain Co^{2+} doped ZnS nanoparticles. Similarly undoped and other transition metal like Fe^{2+} (1.47×10^{-4} mol), Ni^{2+}(1.39×10^{-4} mol) and Mn^{2+}(1.48×10^{-4} mol) doped ZnS nanoparticles were synthesized. To study the effect of zinc salt anions on the final product, we have also synthesized undoped ZnS nanoparticles using $ZnCl_2$ (2.5×10^{-3} mol) instead of the $Zn(NO_3)_2$ as precursor.

4B. 3 Results and discussion

X-ray Powder diffraction (XRD)

The X-ray diffraction (XRD) pattern of undoped and doped ZnS nanoparticles are shown in Figure. 1. The XRD pattern have main diffraction peaks corresponding to (111), (220) and (311) planes indicating zinc blende phase (JCPDS card no. 8000-20). The broadening of XRD peaks indicates particle size in nano-range. Absence of peaks of any other phases confirms the high purity and crystallinity of the as-synthesized

ZnS nanoparticles. On the basis of the full width at half-maximum (FWHM) intensity of the three major XRD peak using Debeye-Scherrer formula [6] the particle size was calculated. The average nanocrystallite size was found to be in the range of 2.0-4.0 nm (Table 4B.1).

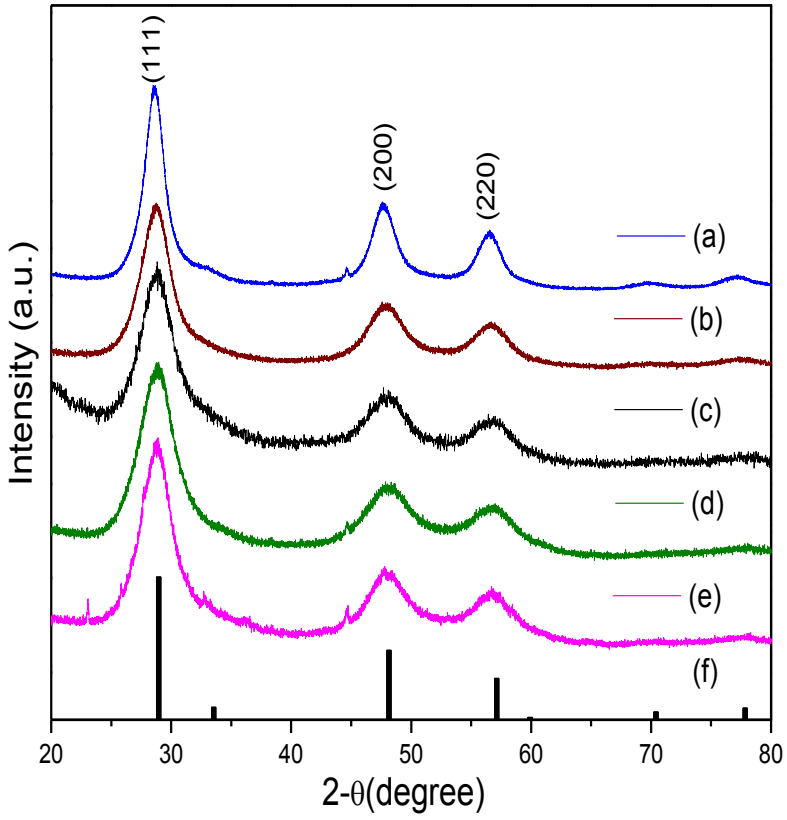

Figure 4B.1. XRD pattern of (a) undoped ZnS (b) ZnS:Fe^{2+} (c) ZnS:Co^{2+} (d) ZnS:Ni^{2+} doped and (e) ZnS:Mn^{2+} nanoparticles (f) Bulk cubic phase ZnS (JCPDS card no.800020).

Presence of dopant ions in the host matrix was analyzed by EDX analysis as shown in Figure 4B.2 and the elemental composition is presented in Table 2. The Zn:S stoichiometric ratio is nearly 1 in the doped and undoped nanoparticles. The EDX analysis confirms the presence of dopant ions in the host matrix.

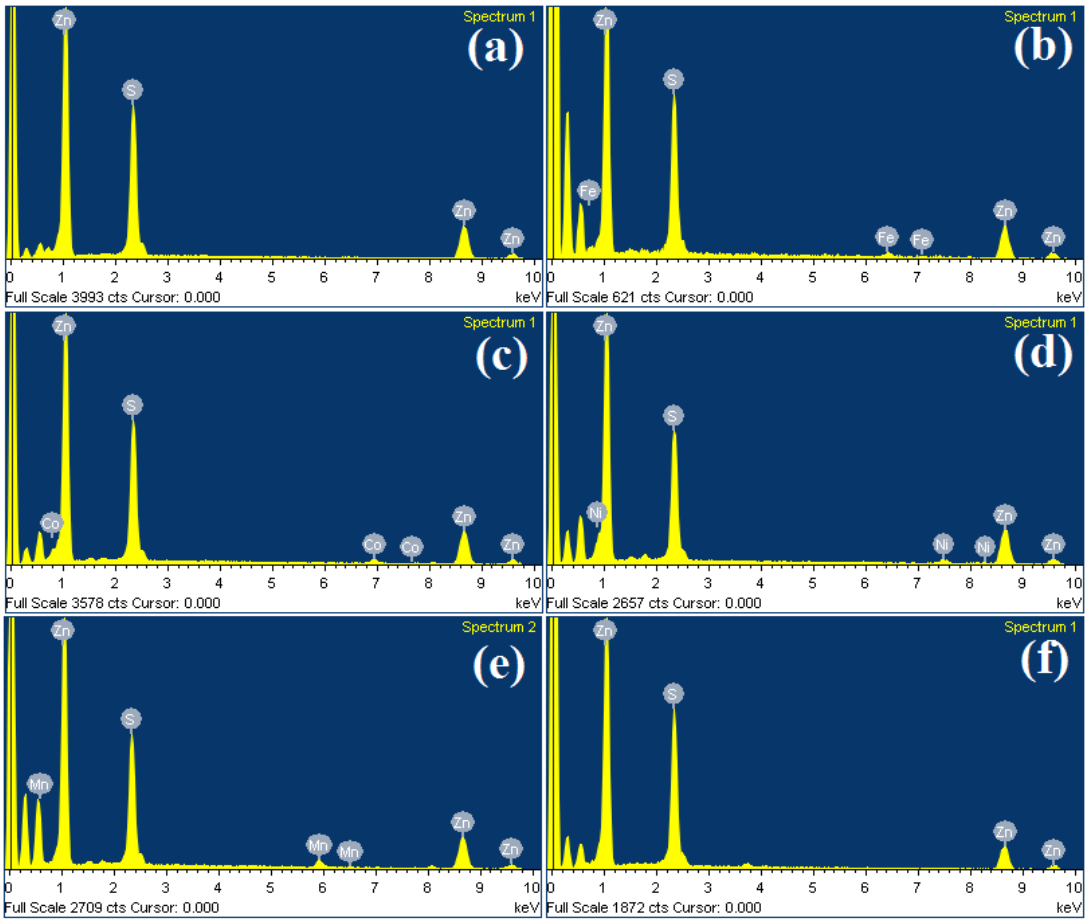

Figure 4B.2. The EDX analysis spectra of (a) Undoped ZnS (NO_3^- salt as precursor) (b) ZnS:Fe^{2+}, (c) ZnS:Co^{2+}, (d) ZnS:Ni^{2+}, and (e) ZnS:Mn^{2+}, (f) ZnS nanoparticles (Cl^- salt as precursor).

Transmission Electron Microscopy (TEM)

The size and shape of the nanoparticles were studied by TEM analysis as shown in Figure. 4B.3 and insets show the selected area electron diffraction (SAED) patterns. For undoped ZnS nanoparticles, nano-aggregates of longest dimension of ~120 nm, composed of small spherical nanoparticles of size 5.8 nm can be observed. Hsiao et al. reported compact aggregates of TiO_2 nanoparticles of size in the range 90-160 nm with a non-uniform shape synthesized by solution-gel method [7]. In case of ZnS:Fe^{2+} similar type of spherical nano-aggregates having average diameter 3.6 nm and size

75.1 nm are formed. Han et al. reported a hollow spherical ZnS microstructures assembled by nanoparticles using solution phase thermalysis of at 80ºC using N, N-dimethylformamide (DMF) as solvent [8].

In case of ZnS:Ni^{2+} spherical nano-aggregates of size 135 nm and diameter 3.3 nm are formed. While for ZnS:Co^{2+}, the same with 122 nm size and 3.8 nm diameter can be observed. The SAED pattern reveals crystalline nature in all the as-synthesized ZnS nanoparticles. Here the surfactant seems to play an important role in controlling the particle size. The morphology of undoped ZnS nanoparticles was also studied SEM (Figure 4). The SEM image shows nearly spherical nanoparticles of average size ~67.8 nm.

The hydrodynamic diameter of the doped and undoped ZnS nanoparticles was studied by dynamic light scattering (DLS) technique. In this technique, the scattering intensity based on Rayleigh scattering [9] is measured which depends on Brownian motion of the dispersed particles in the medium. The particle size measured by this method is considerably larger than the actual size of dried core particle due to contribution of the hydration layer. The hydrodynamic diameters of the as-synthesized nanoparticles are reported in Table 3 and particle size distribution (by intensity) shown in Figure. 4B.5. The hydrodynamic diameter increases in the doped nanoparticles. Undoped ZnS with zinc chloride as a precursor has hydrodynamic diameter of 337.8 nm while those of Fe^{2+}, Co^{2+}, Ni^{2+} and Mn^{2+} doped ZnS nanoparticles are in the range of 300-750 nm.

The surface charge stabilization was studied by zeta potential (ζ). The surface charge varied with the counter anion of metal salts as shown in Table 3. The undoped ZnS nanoparticles synthesized from zinc nitrate and zinc chloride are negatively charged and positively charged respectively. In case of Co^{2+} and Fe^{2+} doped nanoparticles with dopant anion chloride and sulphate respectively, we obtained positive charge. In Ni^{2+} and Mn^{2+} doped ZnS (dopant metal salts were in the acetate form), we obtained negative surface charge of different magnitude. Zeta potential of Ni^{2+}, Mn^{2+}, Co^{2+},

Fe^{2+} doped and undoped ZnS nanoparticles are compared (as shown graphically in Figure. 4B.6). A large variation of the surface charge in the as-synthesized nanoparticles can be observed. A widely cited empirical rule states that electrostatic stabilization requires zeta potential of at least ±30 mV [10]. Exceptions to this rule also exist, Hang et al. reported electrostatic stabilization of barite at zeta potential of ±15 mV [11]. The surface charge stability at low zeta potential indicates some degree of stearic stabilization.

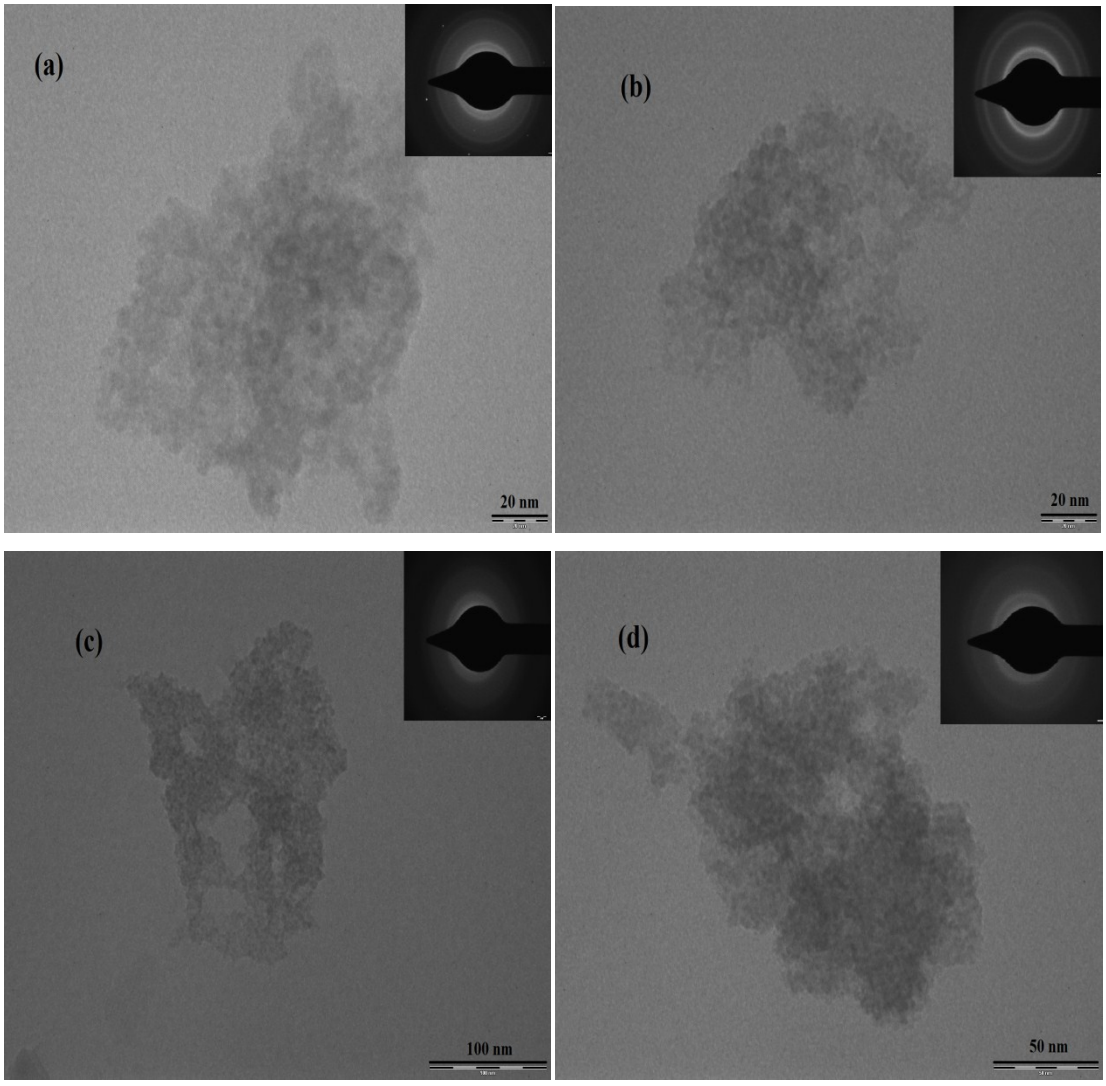

Figure 4B.3 TEM image and inset SAED of (a) undoped ZnS (NO_3^- salt as precursor) (b) $ZnS:Fe^{2+}$ (c)$ZnS:Co^{2+}$ and (d) $ZnS:Ni^{2+}$ nanoparticles.

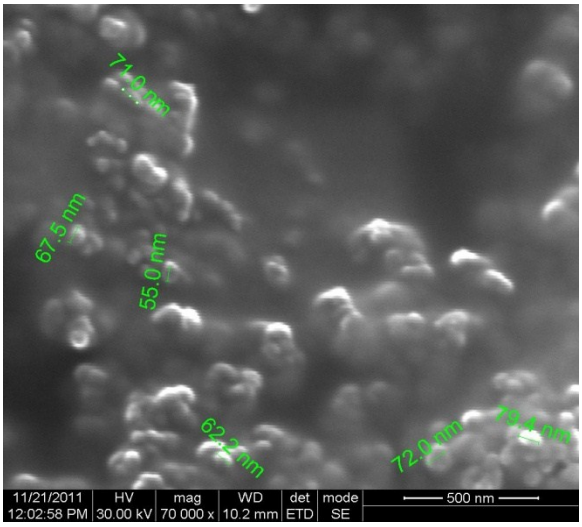

Figure 4B.4 SEM image of undoped ZnS (NO_3^- salt as precursor) nanoparticles.

From this study it is established that the surface charge of the undoped and doped ZnS nanoparticles depends on the surface adsorbed ions and the anions (like acetate and chloride) of the precursor molecules play an important role during growth stage to achieve a stable size. The surface charge can tuned by adjusting different experimental parameters like dopants ions and metal salts.

Table. 4B.1. Absorption edge, band gap energy, particle size by effective mass model and Debye Scherrer formula.

Sample	Absorption edge (nm)	Band gap energy (eV)	Particle size (From UV absorption) R (nm)	Particle size (XRD) D (nm)
Undoped ZnS (NO_3^-)	322	3.86	2.0	3.4
ZnS:Fe^{2+}	315	3.94	1.8	2.5
ZnS: Co^{2+}	315	3.94	1.8	2.8
ZnS: Ni^{2+}	316	3.93	1.9	2.4
ZnS: Mn^{2+}	316	3.93	1.9	2.8
Undoped ZnS (Cl^-)	326	3.81	2.2	-

Table 4B.2. Elementary composition of the doped and undoped ZnS nanoparticles as studied by EDX.

Sample	Amount of Zn doped (at.%)	Amount of S doped (at.%)	Amount of Dopant in ZnS matrix (at.%)
Undoped ZnS (NO_3^-)	50.63	49.37	-
ZnS:Ni	43.07	52.32	4.61
ZnS:Co	45.66	50.96	3.38
ZnS:Mn	42.87	52.52	4.61
ZnS:Fe	49.40	47.20	3.40
Undoped ZnS (Cl^-)	49.13	50.87	-

Table no. 4B.3. Hydrodynamic diameter, zeta potential and corresponding anions of the metal salt used for the synthesis of doped and undoped ZnS nanoparticles.

Sample	Hydrodynamic diameter (nm)	Zeta potential (mV)	Zn salt anion	Dopant anion
Undoped ZnS (NO_3^-)	118.0	-13.06	NO_3^-	-
ZnS:Fe^{2+}	337.1	+6.63	NO_3^-	SO_4^{2-}
ZnS: Co^{2+}	451.9	+10.36	NO_3^-	Cl^-
ZnS: Ni^{2+}	598.9	-13.04	NO_3^-	Ac
ZnS: Mn^{2+}	743.3	-5.68	NO_3^-	Ac
Undoped ZnS (Cl^-)	337.8	+9.06	Cl^-	-

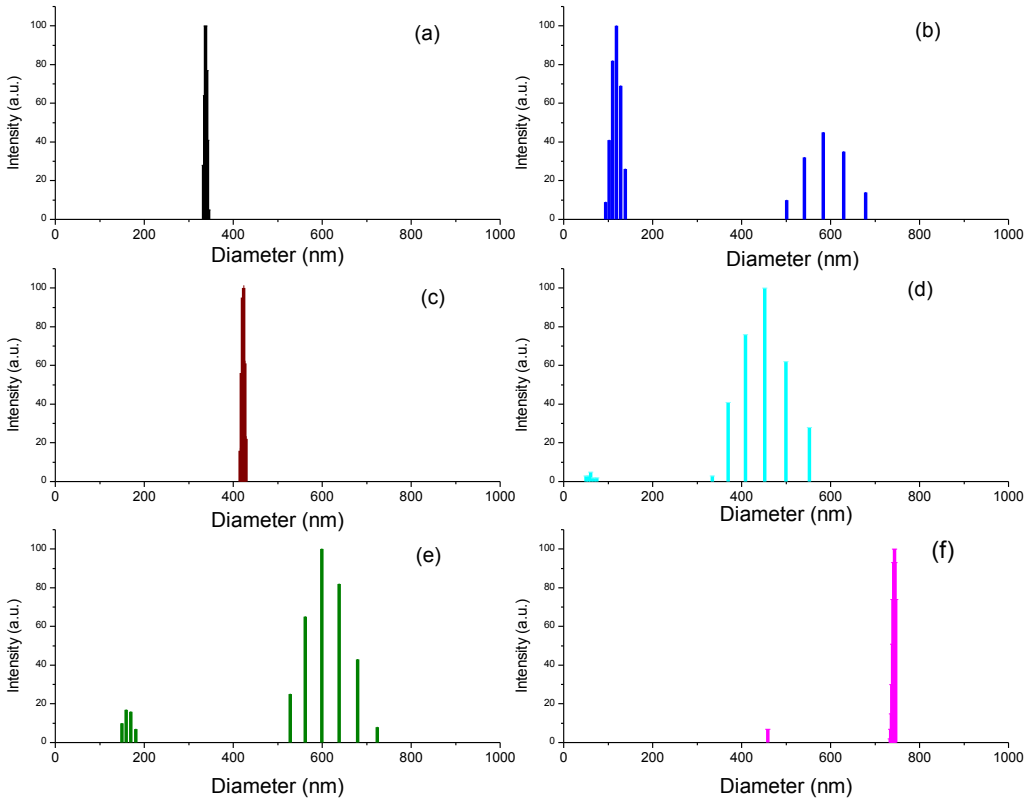

Figure 4B.5. Hydodynamic diameter using DLS of (a) undoped ZnS (Cl^- salt as precursor) (b) undoped ZnS (NO_3^- salt as precursor) (c) ZnS:Fe^{2+} (d) ZnS:Co^{2+} (e) ZnS:Ni^{2+} and (f) ZnS:Mn^{2+}.

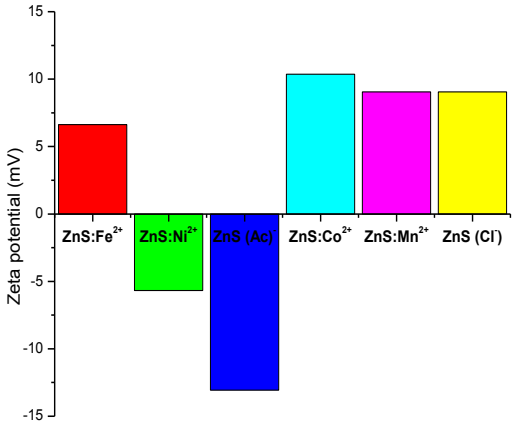

Figure 4B.6. Comparision of the zeta potential values of different doped and undoped ZnS nanoparticles (synthesized using precursor salt).

Optical study

The optical absorption spectra of the nanoparticles were measured in the range of 200-400 nm as shown in Figure. 4B.7. The doped nanoparticles show the absorption edge at 315 nm while that of undoped at 322 nm. The absorption peaks are blue shifted and band gap energy increases compared to the bulk ZnS (335nm and 3.7 eV) [12]. This is due to quantum confinement effect [13]. The particle sizes as calculated using effective mass model [14], were in the range of 1.8-2.2 nm as given in the table. 1. The band gap energy of doped and undoped ZnS nanoparticles (as given in table. 1) increased when compared with that of bulk ZnS material (3.7 eV).

The photoluminescence emission spectra of the as-synthesized nanoparticles are shown in Figure. 4B.8. ZnS:Fe^{2+}, ZnS:Ni^{2+} and ZnS:Mn^{2+} nanoparticles show emission at (330 nm and 350 nm) while ZnS:Co^{2+} at 350 nm. The band at 330 nm can be attributed to the near-band edge emission [15]. The undoped ZnS nanoparticles show emission band around 350 nm. This band can be attributed to the near band to band transitions [16]. The undoped ZnS nanoparticles synthesized with nitrate salt showed highest intensity of emission in the UV region when compared with the doped and undoped (Cl^- salt) ZnS nanoparticles.

The ZnS:Ni^{2+} doped nanoparticles show broad blue emission band around 440 nm. Denzler et al. have attributed the emission at 440 nm due to the transitions from Zn vacancy states [17]. A weak emission band around 470 nm was observed in the doped and undoped ZnS nanoparticles. Chai et al. reported a weak band around 465 nm arises from the surface states and the large surface-to-volume ratio in nanoparticles [18]. Similarly the band around 470 nm due to large surface-to-volume ratio of nanoparticles. The PL study shows that the PL emission of ZnS nanoparticles can be modified by addition of different transition metal ions as dopant in the host matrix.

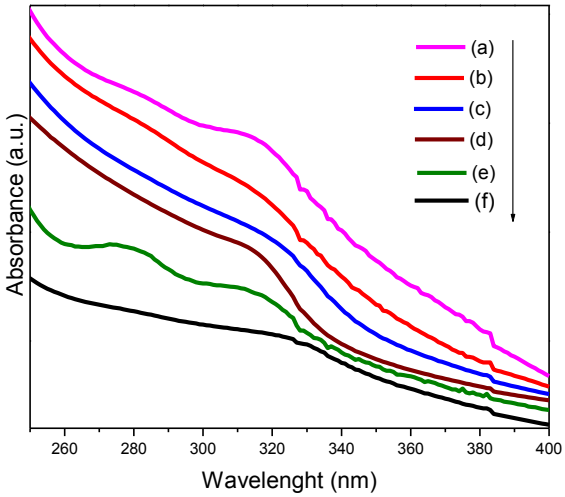

Figure 4B.7 Absorption spectra of (a) ZnS:Mn^{2+} nanoparticles (b) ZnS:Co^{2+} (c) undoped ZnS (using NO_3^- salt as precursor) (d) ZnS:Fe^{2+} (e) ZnS:Ni^{2+} and (f) undoped ZnS (using Cl^- salt as precursor).

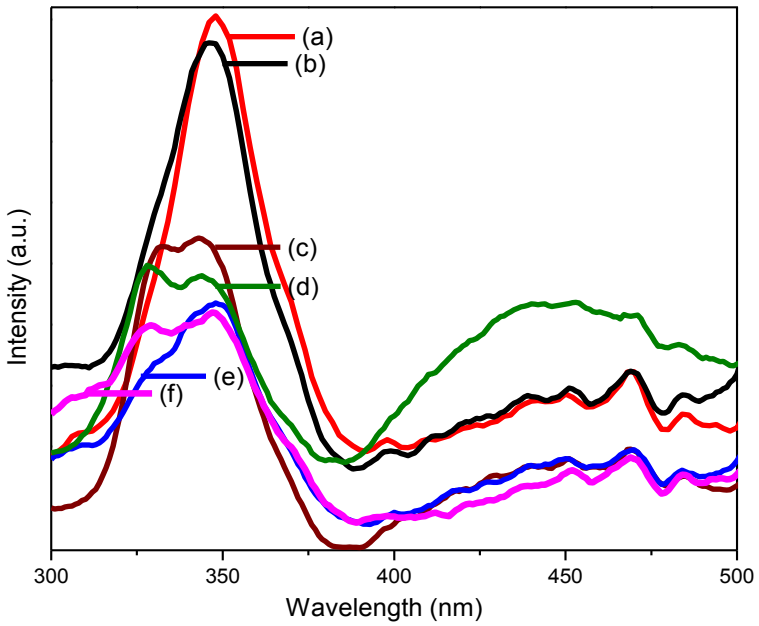

Figure 4B.8 PL spectra of ZnS with different dopant ions (a) undoped ZnS (using NO_3^- salt as precursor) (b) undoped ZnS (using Cl^- salt as precursor) (c) ZnS:Fe^{2+} (d) ZnS:Ni^{2+} (e) ZnS:Co^{2+} and (f) ZnS:Mn^{2+} nanoparticles.

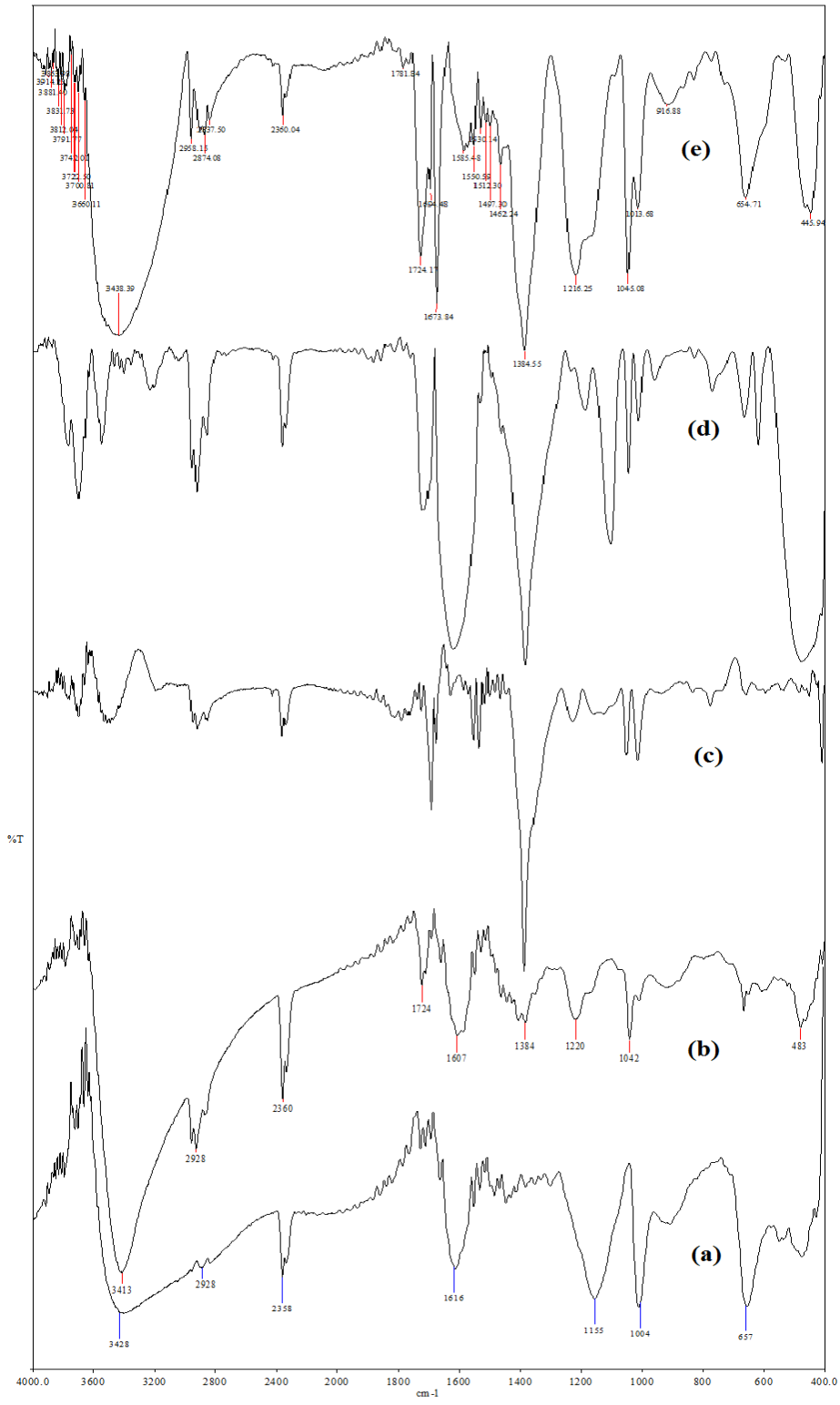

Figure 4B.9. FTIR spectra of AOT capped (a) undoped ZnS (using NO_3^- salt as precursor) (b) ZnS:Co^{2+} nanoparticles (c) ZnS:Fe^{2+} nanoparticles (d) ZnS:Mn^{2+} nanoparticles and (e) ZnS:Ni^{2+} nanoparticles.

Fourier Transform Infrared Spectroscopy (FT-IR)

The presence of AOT surfactant as a surface capping agent was confirmed by FTIR spectroscopy. The FTIR spectrum of AOT capped doped and undoped ZnS nanoparticles are shown in Figure. 4B.9. The peak at 657 cm^{-1} corresponds to the vibration of Zn–S [19]. The peak at 1155 cm^{-1} and 1220 cm^{-1} in undoped and ZnS:Co^{2+} nanoparticles respectively corresponds to C–O stretching of AOT. The peak at 1732 cm^{-1} and 1724 cm^{-1} in undoped and ZnS:Co^{2+} nanoparticles respectively corresponds to the carbonyl stretching peak of AOT. The peak at 1737 cm^{-1} corresponds to the carbonyl stretching peak of AOT system [20]. The peak at 2928 cm^{-1} corresponds to C–H stretching vibration in undoped and ZnS:Co^{2+} nanoparticles. The broad peak around 3400 cm^{-1} can be assigned to O–H stretching. From the FTIR spectra we can consider that AOT was adsorbed on the surface of nanoparticles.

Conclusion

We have successfully synthesized Fe^{2+}, Co^{2+}, Ni^{2+} , Mn^{2+} doped and undoped ZnS nanoparticles by using simple oil-in-water (o/w) microemulsion method. The XRD pattern revealed that nanoparticles exhibited zinc blende structure. TEM analysis showed that nanoaggregates were made up of monodispersed spherical nanoparticles of size in the range of 3.0-6.0 nm. The surface stabilization was studied by zeta potential, which showed different precusor anions play an important role in the surface charge stabilization of the nanoparticles. Photoluminesence study showed emission bands in the UV and blue regions. Undoped ZnS nanoparticles showed high intensity of the PL emission in the UV region and ZnS:Ni^{2+} showed high PL intensity in the visible range. The PL study shows that these doped and undoped nanoparticles may find applications in future optical nanodevices.

References

[1] L.E. Greene, M. Law, J. Goldberger, F. Kim, J.C. Johnson, Y. Zhang, R.J. Saykally, P. Yang, *Angew. Chem. Int. Ed.* **2003,** 42, 3031.

[2] J. Xu, Y. Li, *J. Colloid Interface Sci.* **2003,** 259, 275.

[3] C. Bi, L. Pan, M. Xu, J. Yin, L. Qin, J. Liu, H. Zhu, J.Q. Xiao, *Mater. Chem. Phys.* **2009,** 116, 363.

[4] T. Kang, J. Sung, W. Shim, H. Moon, J. Cho, Y. Jo, W. Lee, B. Kim, *J. Phys. Chem. C* **2009,** 113, 5352.

[5] F. Li, Y. Ding, P. Gao, X. Xin, Z. L. Wang, *Angew. Chem. Int. Ed.* **2004**, 43, 5238.

[6] R. Jenkins, R.L. Snyder, *Introduction to X-ray powder diffractometry*, John Wiley and sons. NewYork, **1996**.

[7] I.-L. Hsiao, Y.-J. Huang, Chem. Res. Toxicol. **2011,** 24, 303.

[8] Q. Han, F. Qiang, M. Wang, J. Zhu, L. Lu, X. Wang, *Mat. Res. Bull.* **2010,** 45, 813.

[9] J. Holoubek *J. Quantitative Spectroscopy & Radiative Transfer* **2007,** 106, 104.

[10] J.M. Berg, A. Romoser, N. Banerjee, R. Zebda, C.M. Sayes, *Nanotoxicology* **2009,** 3, 276.

[11] J. Hang, L. Shi, X. Feng, L. Xiao, *Powder Technol.* **2009,** 192, 166.

[12] Y.C. Li, X.H. Li, C.H. Yang, Y.F. Li, *J. Phys. Chem. B* **2004,** 108, 16002.

[13] R. Rossetti, R. Hull, J.M. Gibson, L.E. Brus, *J. Chem. Phys.* **1985,** 82, 552.

[14] Y. Kayanuma, *Phys. Rev. B* **1988**, 38, 9797.

[15] J.X. Ding, J.A. Zapien, W.W. Chen, Y. Lifshitz, S.T. Lee, X.M. Meng, *Appl. Phys. Lett.* **2004,** 85, 2361.

[16] N. Chestnoy, R. Hull, L.E. Brus, *J. Chem. Phys.* **1986,** 85, 2237.

[17] D. Denzler, M. Olschewski, K. Sattler, *J. Appl. Phys.* **1998,** 84, 2841.

[18] L. Chai, J. Du, S. Xiong, H. Li, Y. Zhu, Y. Qian, *J. Phys. Chem. C* **2007,** 111, 12658.

[19] Z. Rui, L. Yingbo, S. Shuqing, *Opt. Mater.* **2012,** 34, 1788.

[20] Y. Luan, G. Xu, G. Dai, Z. Sun, H. Liang, *Colloid Polym. Sci.* **2003,** 282, 110.

4C.1 Introduction

There are two types of microemulsions, oil-in-water (O/W) and water-in-oil (W/O) type. The water-in-oil (W/O), also known as reverse micelle (RM) system (soft mater), is one of the commonly used approach for synthesizing nanoparticles.

Reverse micelles (RMs) are formed when a small amount of water is added to a mixture of a suitable surfactant in nonpolar solvent(s) as oil phase. RMs are widely utilized as media to prepare inorganic nanomaterials. The reverse micellar method allows the flexibility to control the size and shape along with monodispersity of nanostructures. The soft chemistry is easy to handle, simple and require no extreme temperature or pressure control.

Reverse microemulsion is a thermodynamically stable phase separation of water-in-oil, stabilized by a surfactant in which surfactant shell and water-droplet cores constitute micelles with radii in range of 5 to 100 nm [1]. The size and shape of the nanoparticles can be tailored by varying the micelle forming parameters during the reaction [2]. The formation of monodispersed ZnS and ZnO nanoparticles is one of the challenges for the researchers. Micelles can be used as nano reactors as reported earlier [3]. Lv et al. synthesized ZnS nanowires using sodium bis(2-ethylhexyl)sulfosuccinate (AOT) reverse micelles [4]. Xu et al. synthesized ZnS nanorods using Triton X-100 or CTAB/cyclohexane/water microemulsion [5].

In present work, we have synthesized ZnS and ZnO nanoparticles using AOT/Iso-octane/water (at different water to surfactant ratio (ω)) and ZnO nanorods in (CTAB/1-butanol/cyclohexane/Aqueous solution) reverse micelle respectively. The optical property of the as-synthesized nanoparticles has been studied.

4.C.2 Experimental

(a) Materials

Analytical Grade zinc nitrate $Zn(NO_3)_2$, sodium sulphide $Na_2S.xH_2O$, iso-octane, sodium bis(2-ethylhexyl)sulfosuccinate (AOT) $\{NaO_3SCH(COOC_8H_{17})CH_2COOC_8H_{17}\}$, cetyltrimethylammonium bromide (CTAB), cyclohexane, 1-butanol, sodium hydroxide were purchased from SD Fine Chemie Pvt. Ltd. Mumbai, India and used as received.

(b) Synthesis of ZnS nanoparticles

A microemulsion of Zn^{2+} ion was prepared, by mixing aqueous solution of (2.2 ml (0.05M zinc nitrate)), 3.4 g of AOT and Iso-octane (6.4 ml). The water to surfactant ratio (ω) was 15.96 using sodium bis(2-ethylhexyl)sulfosuccinate (AOT) as surfactant [6]. Similarly S^{2-}(0.05M) ions containing microemulsion was prepared using above method. To the Zn^{2+} ion containing microemulsion S^{2-}(0.05M) ions containing microemulsion was added drop wise. The reaction mixture was stirred for 48h. The reaction mixture was centrifuged, followed by several washing with ethanol. The product was dried at 60°C. Similarly, ZnS nanoparticles were synthesized using ω= 12.34.

(c) Synthesis of ZnO nanoparticles

In a round bottom flask 1.579 g of CTAB, 1-butanol (1.6 ml) and cyclohexane (8.0 ml) were mixed [7]. Then 0.94 ml of aqueous solution of Zn^{2+} (0.05M) was introduced dropwise and stirred for 1 hr. Similarly NaOH (0.2 M) containing microemulsion was prepared using above method. Then microemulsion containing aqueous solution of NaOH was added drop wise. The reaction mixture was allowed to stir for 24 h and centrifuged at 10,000 rpm. The product was washed with water several times and dried at 100°C.

4.C.3 Results and discussion

(A) ZnS nanoparticles using AOT as surfactant

Transmission Electron Microscopy (TEM)

The size and morphology of as-synthesized nanoparticles were studied by TEM as shown in Figure 4C.1. The ZnS nanoparticles synthesized in reverse micelle with ω=15.96 form nano-aggregates composed of monodispersed spherical nanoparticle of size 4.2 nm while with ω=12.34 form the same morphology with reduced size of spherical nanoparticles of 3.6 nm size. Hence the size of reverse micelle is linearly dependent on the ratio of water to surfactant concentration (ω) [8]. Tai et al. reported increase in the particle size of $CaCO_3$ nanoparticles with increase in the ω value [6]. Ranjan et al. also reported increase in particle size of cupper oxalate with increase in ω value. They explained this on the basis of increase in the flexibility of the surfactant film with increasing aqueous content, which results in a higher intermicellar exchange rate [9].

Dynamic light scattering (DLS)

The hydrodynamic diameters of the as-synthesized nanoparticles were measured by dynamic light scattering (DLS) technique as shown in Figure 4C.3 and Table 1. The DLS measures the intensity of the scattered light from particles dispersed in a solvent and are in a continuous motion due to the Brownian movement. The hydrodynamic diameter of ZnS nanoparticles synthsized with ω value 15.96 and 12.34 are 601 and 301 nm respectively indicating decrease in hydrodynamic diameter with decrease in ω value.

Optical study

The UV absorption of the as-synthesized ZnS nanoparticles is shown in Figure 4C.2. The absorption edge of the ZnS nanoparticles showed a blue shift when compared to the bulk material. The blue shift of the absorption edge is due to quantum confinement [10].

The photoluminescence spectra of the as-synthesized ZnS nanoparticles are shown in Figure 4C.4. A broad band centered at about 340 nm is due to band to band transitions when ω=15.96 [11] and the same is 5 nm blue shifted (335 nm) when ω=12.34. The emission band at 400 nm, common for both ω values, is due to the recombination of electrons from the energy level of sulfur vacancies (neutral donor) with the holes from the valence band [12]. The broad emission band at 410 nm is due to the defects present in the material. The high intensity of this band for ω=15.96 indicate presence of more number of defects in the material.

Table 4C.1. Hydrodynamic diameter and absorption edge of as-synthesized ZnS nanoparticles.

water to surfactant ratio (ω)	Hydrodynamic diameter (nm)	Absorption edge (nm)
15.96	621.8	311.1
12.34	301.4	310.7

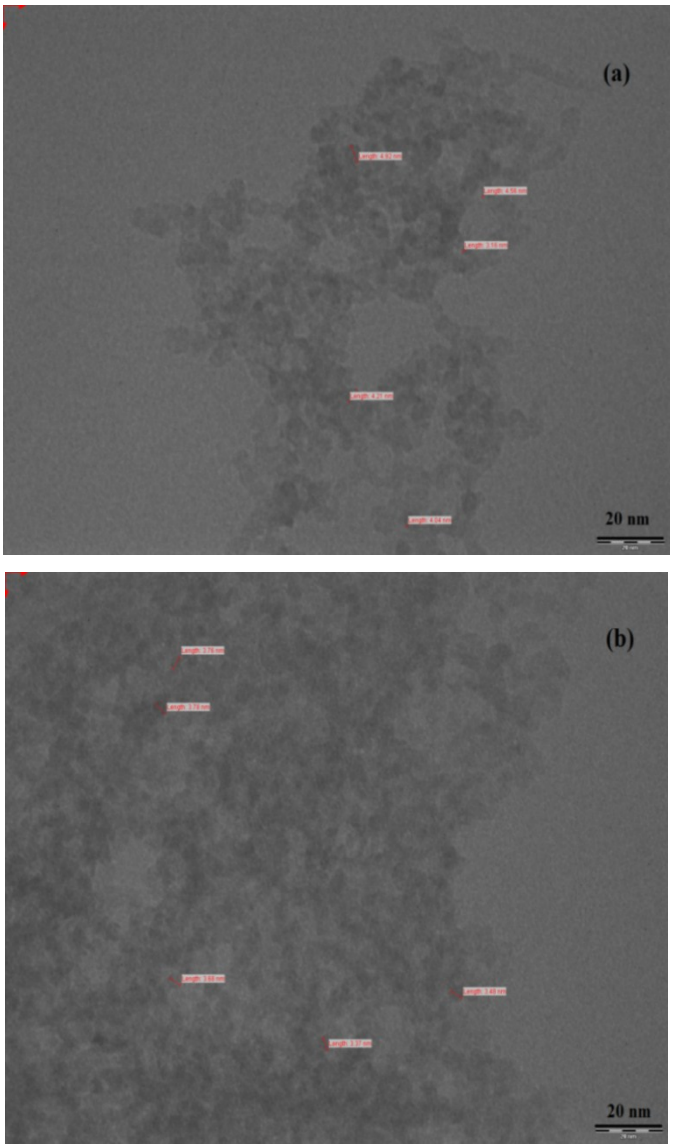

Figure 4C.1. TEM images of ZnS nanoparticles synthesized in microemulsion of (a) ω=15.96 and (b) ω=12.34.

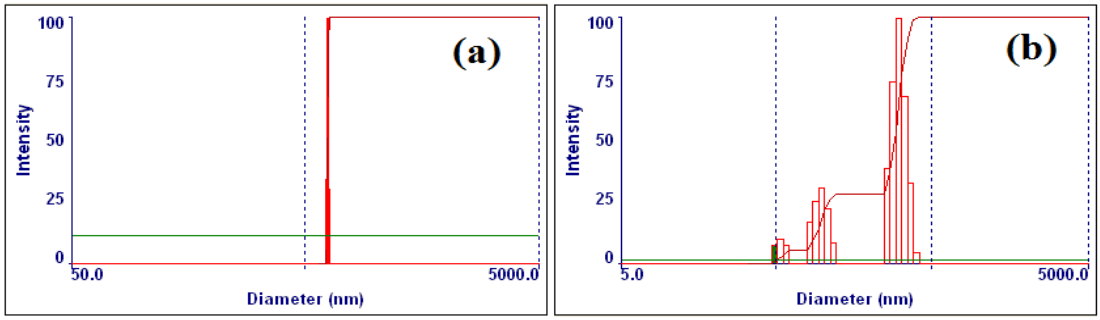

Figure 4C.2. Hydrodynamic diameter of ZnS NPs synthesized in (a) ω=15.96 and (b) ω=12.34.

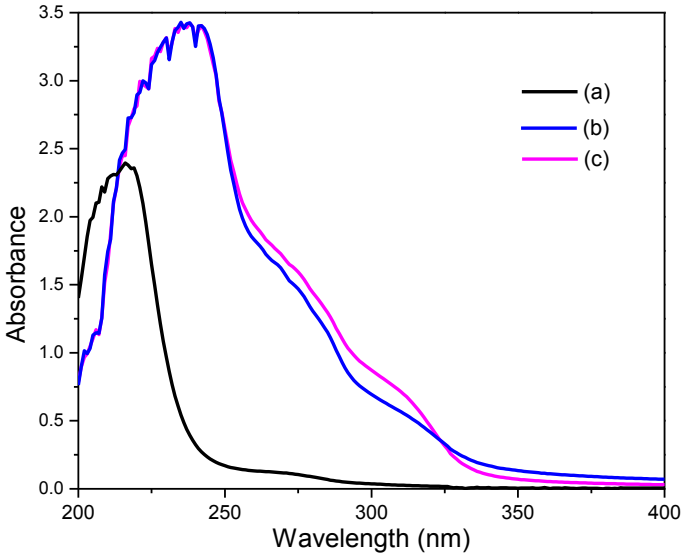

Figure 4C.3. UV absorption spectra of ZnS NPs samples synthesized in (a) Aot solution (b) ω=15.96 (c) ω=12.34.

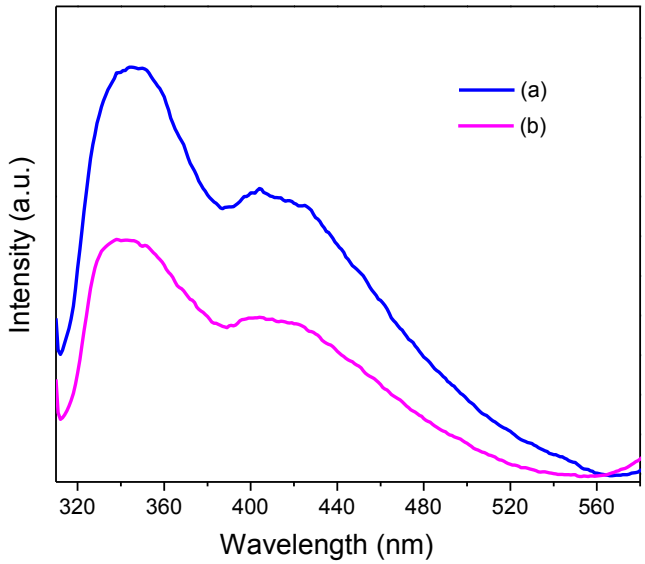

Figure 4C.4. Photoluminescence of the ZnS nanoparticles synthesized in (a) ω=15.96 (b) ω=12.34.

(B) ZnO nanorods using CTAB as surfactant

Transmission Electron Microscopy (TEM)

The size and morphology of as-synthesized ZnO nanoparticles was studied by TEM as shown in Figure 4C.5. Nanorods of length ~1.8 μm and width ~178 nm can be observed.

Dynamic light scattering (DLS)

The hydrodynamic diameter of ZnO nanoparticles was studied by DLS technique. The hydrodynamic diameter is 748.1 nm. The particle size distribution reveals monodispersed particle size as shown in Figure 4C.6.

Optical properties

The absorption spectrum of ZnO nanorods is shown in Figure 4C.7. The ZnO nanorods show absorption at 366 nm which is blue shifted when compared to the bulk ZnO material (388 nm) due to quantum confinement.

The PL emission spectrum of ZnO nanorods is shown in Figure 4C.8. A sharp emission peak at 400 nm was observed, which can be attributed to the direct recombination of photogenerated charge carriers (excitation emission) [13]. Broad emission bands at 514 nm and 535 nm were observed. The emission in the green region is due to existence of oxygen vacancies on the ZnO surface [14].

Fourier Transform Infrared Spectroscopy (FT-IR)

The presence of CTAB as a capping agent was confirmed by FTIR spectroscopy as shown in Figure 4C.5. A peak at 435 cm^{-1} can be assigned to stretching of Zn-O bond [15]. A peak at 670 cm^{-1} can be assigned to methylene rocking. A peak at 1117 cm^{-1}

can be assigned to C-C-N asymmetric stretching mode. A peak at 1383 cm^{-1} can be assigned to the adsorbed nitrate ions on the ZnO nanoparticles. A peak at 2363 cm^{-1} can be assigned to adsorbed CO_2. A peak at 2851 cm^{-1} and 2920 cm^{-1} indicates methylene symmetric and asymmetric C-H stretching. A broad peak at 3397 cm^{-1} can be due to adsorbed moisture.

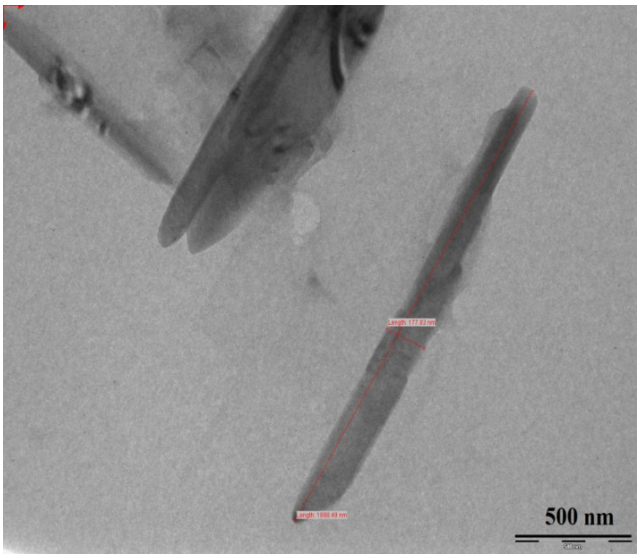

Figure 4C.5. TEM image of ZnO reverse micelle nanoparticles synthesized in CTAB/1-butanol/cyclohexane/Aqueous system.

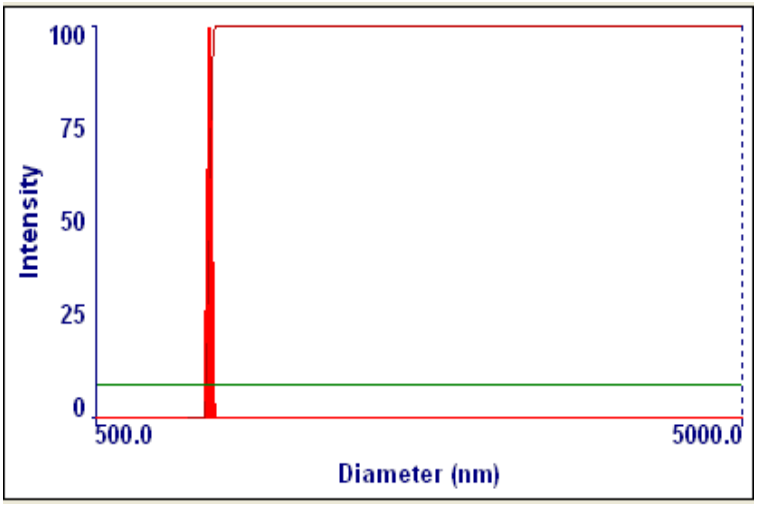

Figure 4C.6. Hydrodynamic diametet of ZnO nanoparticles synthesized in CTAB/1-butanol/cyclohexane/Aqueous system.

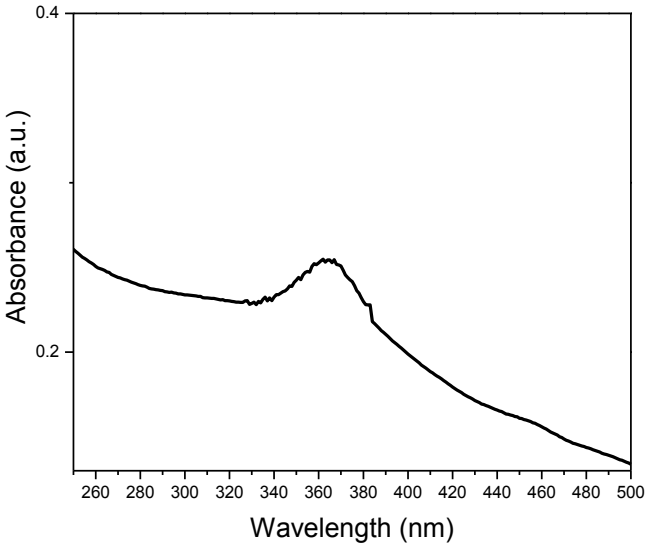

Figure 4C.7. Absorption spectra of ZnO nanoparticles synthesized in CTAB/1-butanol/cyclohexane/Aqueous system.

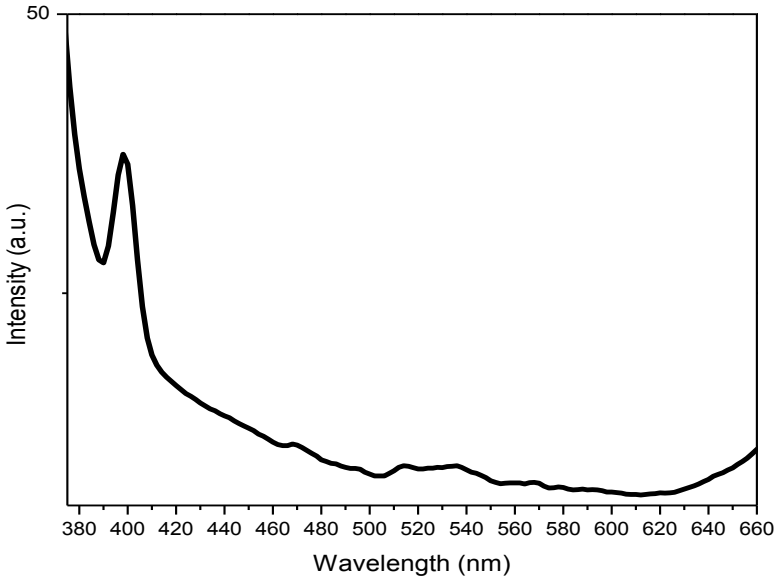

Figure 4C.8. Photoluminescence emission spectra of ZnO synthesized in CTAB/1-butanol/cyclohexane/Aqueous solution.

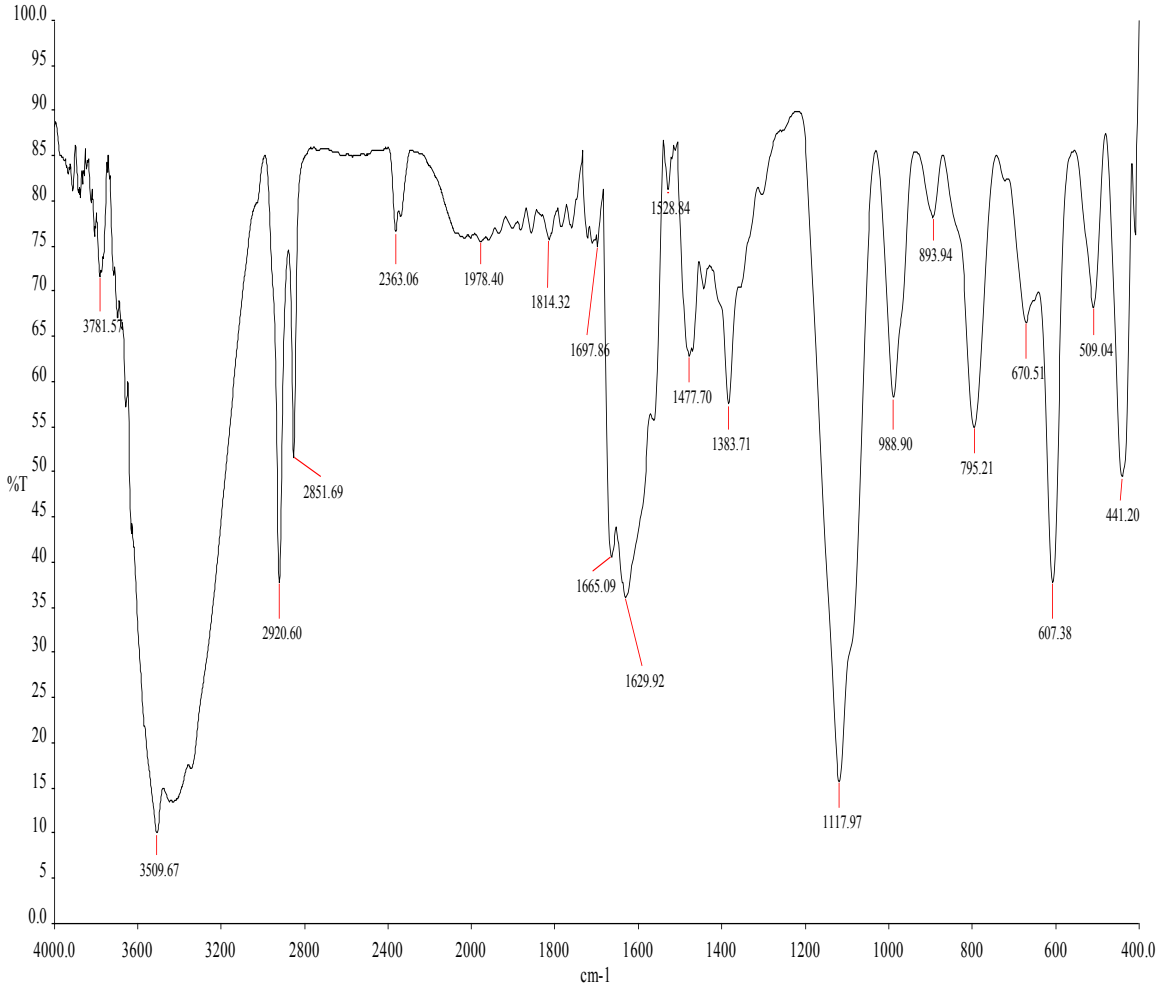

Figure 4C.9 FTIR Spectra of ZnO nanoparticles synthesized in ZnO nanoparticles CTAB/1-butanol/cyclohexane/Aqueous solution.

Conclusion

We have successfully synthesized ZnS nanoparticles and ZnO nanoparticles by using reverse micelle technique. The particles size of ZnS nanoparticles were in the range of 2.0-4.0 nm were observed by TEM. We can tune the particle size of nanoparticles by changing water to surfactant ratio. The PL emission of ZnS nanoparticles showed two emission bands 340 nm and 410 nm. The ZnS nanoparticles synthesized in ω=15.96 showed high PL emission intensity. The PL study of ZnO nanorods showed emission peak at 400 nm. The optical properties show that these nanoparticles can find application in optical devices.

References

[1] M.P. Pilieni *Nature* **2003**, 2, 145.

[2] C.M. Bender, J.M. Burlitch, D. Barber, C. Pollock, *Chem. Mater.* **2000**, 12, 1969.

[3] S.G. Dixit, A.R. Mahadeshwar, S.K. Haram, *Colloids Surf.* A **1998,** 133, 69.

[4] R.T. Lv, C.B. Cao, H.S. Zhu, *Mater. Res. Bull.* **2004,** 39, 1517.

[5] J. Xu, Y. Li, *J. Colloid Interface Sci.* **2003,** 259, 275.

[6] C.Y. Tai, C.-K. Chen, *Chemicl engineering Science* **2008,** 63, 3632-3642.

[7] S. Vaidya, P. Rastogi, S. Agarwal, S.K. Gupta, T. Ahmad, A.M. Antonelli, Jr., K. V. Ramanujachary, S.E. Lofland, A.K. Ganguli, *J. Phys. Chem. C* **2008**, 112, 12610.

[8] M. P. Pileni, T. Zemb, C. Petit, *Chem. Phys. Lett.* 118, **1985**, 414.

[9] R. Ranjan, S. Vaidya, P. Thaplyal, M. Qamar, J. Ahmed, A.K. Ganguli, *Langmuir* **2009**, 25, 6469.

[10] R. Rossetti, R. Hull, J.M. Gibson, L.E. Brus, *J. Chem. Phys.* **1985,** 82, 552.

[11] J.X. Ding, J.A. Zapien,W.W. Chen, Y. Lifshitz, S.T. Lee, *Appl. Phys. Lett.* **2004,** 85, 2361.

[12] W.G. Becker, A.J. Bard, *J. Phys. Chem.* **1983**, 87, 4888.

[13] D.W. Bahnemann, C. Kormann, M.R. Hoffmann, *J. Phys. Chem.* **1987**, 91, 3789.

[14] A. van Dijken, E.A. Meulenkamp, D. Vanmaekelbergh, A. Meijerink, *J. Lumin.* **2000**, 87-9, 454.

[15] S. Maensiri, P. Laokul, V. Promarak, *J. Cry. Growth* **2006,**289, 102.